Angewandte Chemie
Eine Zeitschrift der Gesellschaft Deutscher Chemiker

Supporting Information

© Wiley-VCH 2015

69451 Weinheim, Germany

Functionalization of Liquid-Exfoliated Two-Dimensional 2H-MoS_2**

*Claudia Backes, Nina C. Berner, Xin Chen, Paul Lafargue, Pierre LaPlace, Mark Freeley, Georg S. Duesberg, Jonathan N. Coleman, and Aidan R. McDonald**

anie_201409412_sm_miscellaneous_information.pdf

Contents

Experimental Details 2
Variation of sonication conditions 5
Stability of the dispersions after functionalization 6
X-ray photoelectron spectroscopy 8
Zeta Potential 15
DRIFT IR spectroscopy 16
Thermogravimetric analysis 17
IR and Raman spectroscopy after TGA 19

Experimental Details

Materials

2H-MoS_2 powder (6 μm particle size), $Cu(OAc)_2$ (anhydrous, purity 98 %), $Ni(OAc)_2$ (anhydrous, >99% purity), $Zn(OAc)_2$ (anhydrous, 99,99% purity), IPA (99.7 % purity), NMP (99% purity), acetone (>99.8 % purity) were purchased from Sigma Aldrich. All chemicals were used as received without further purification.

Sample preparation

For the initial exfoliation, 2H-MoS_2 powder (initial concentration 20 mg/mL) was sonicated for 5 h (60 % amplitude, 6 s pulse on, 2 s pulse off) under ice-cooling using a flathead sonic tip (Sonics VX-750) in 100 mL 2-propanol. The resultant raw dispersion was centrifuged for 90 min at 1500 rpm (240 *g*, Hettich Mikro 22R centrifuge equipped with a fixed angle rotor 1016) to remove unexfoliated 2H-MoS_2. The supernatant was decanted and used for further functionalization, the sediment discarded or re-used for further exfoliation. Typical 2H-MoS_2 concentrations obtained were 32 μg/mL (0.2 mM). Unless otherwise noted, 10 mL of the dispersion were mixed with 10 mL of $M(OAc)_2$ in 2-propanol (10 mM). Each aliquot was subjected to a second sonication (30 min, pointprobe tip, 40 % amplitude, 4 s pulse on, 4 s pulse off, ice-cooling) to achieve functionalization. We note that the 2H-MoS_2 is not long term stable in 2-propanol so that the functionalization was performed immediately after the initial exfoliation. To obtain functionalized 2H-MoS_2 powder for redispersion experiments and IR spectroscopy, the resultant dispersions were subjected to high-speed centrifugation to completely sediment all 2H-MoS_2 and salt associated with it (30 min., 11000 rpm = 13250 *g*, Heraeus Megafuge 16 benchtop centrifuge equipped with a fiberlite rotor F15-6x100). The supernatant containing unbound salt was decanted, the 2H-MoS_2 sediment was reaggitated with fresh 2-propanol and subjected to further high-speed centrifugation (30 min., 11000 rpm = 13250 *g*, Heraeus Megafuge 16 benchtop centrifuge equipped with a fiberlite rotor F15-6x100). This washing procedure is repeated in total three times to remove as much physisorbed and unbound salt as possible. After the final washing step, the sediment was collected with as little 2-propanol as possible (2-3 mL), the solvent was evaporated and the dried material collected.

Characterization

Optical extinction spectra were measured on a Varian Cary 5000 in quartz cuvettes with a path-length of 0.4 cm.

X-ray Photoelectron Spectroscopy was performed under ultra-high vacuum conditions ($< 5\times10^{-10}$ mbar) on two different systems. Most spectra were taken on a VG Scientific ECSAlab Mk II system using Al Kα X-rays (1486.6 eV). The analyzer pass energy was set to 100 eV for survey and 20 eV for core-level spectra, yielding a maximum energy resolution of ~1.2 eV. More highly resolved spectra were taken using monochromated Al Kα X-rays from an Omicron XM1000 MkII X-ray source and an Omicron EA125 energy analyzer. An electron flood gun was used for charge compensation in both cases and the binding energy scale was referenced to the adventitious carbon 1s core-level at 284.8 eV. After subtraction of a Shirley background and the satellite peaks (if applicable), the core-level spectra were fitted with Gaussian-Lorentzian line shapes using the software CasaXPS. Relative atomic percentages were calculated from the ratios of the peak areas after normalization using the relative sensitivity factors (R.S.F.) as provided by the CasaXPS software. Samples were prepared by vacuum-filtering the dispersions using porous cellulose filter membranes (MF-Millipore membrane, mixed cellulose esters, hydrophilic, 0.025 μm, 47 mm) to give thin films.

DRIFT-IR spectra were acquired using a Perkin Elmer Frontier spectrometer equipped with a diffuse reflectance unit. Samples were prepared by grinding the (functionalized) 2H-MoS_2 powder in a CsI (Sigma Aldrich, 99.9 % purity) matrix to yield a grey mixture. The CsI baseline was subtracted from the spectra. All spectra were baseline corrected after acquisition.

Raman spectroscopy was performed using a Horiba Scientific LabRam HR with a 532 nm excitation laser in air under ambient conditions. 10% of the laser power was used corresponding to ~ 2 mW. The Raman emission was collected by a 100× objective (N.A. = 0.8) and dispersed by 1800 lines mm^{-1} grating. The mean of 100 spectra is displayed.

Tapping-mode atomic force microscopy (AFM) was carried out on a Veeco Nanoscope-IIIa (Digital Instruments) system after drop-casting the sample on pre-heated Si/SiO_2 wafers. The number of layers was obtained by dividing the measured height by 1.9 nm as this was previously determined to be the apparent height of one layer from solution-exfoliated MoS_2.[1]

Thermogravimetric analysis (TGA) was carried out on a Perkin Elmer Pyris thermogravimetric analyzer with the following programmed time-dependent temperature profile: 25-500 °C with 10 K/min. gradient. The initial sample weights were about 0.5 mg, and the experiments were performed under He gas flow.

Zeta potential measurements were carried out on a Malvern Zetasizer Nano system with irradiation from a 633 nm He-Ne laser. Due to the generally lower electrophoretic mobility on solvents compared to aqueous media, a dip cell was used for the measurement. The electrophoretic mobility (μ) was measured using a combination of electrophoresis and laser Doppler velocimetry techniques. The electrophoretic mobility relates the drift velocity of a colloid (ν) to the applied electric field (E); $\nu = \mu E$. All measurements were conducted at 20 °C. The zeta potential ζ is related to the measured electrophoretic mobility μ according to the Smoluchowski approximation. The mean of 5 measurements is displayed.

Variation of sonication conditions

The sonication applied during the functionalization procedure with the pointprobe sonic tip produces material with a high degree of surface functionalization. However, it suffers from the disadvantage of low volume (20-25 mL) thus producing only small quantities of functionalized material. We have therefore tested whether a similar degree of functionalization can be achieved when sonicating with a flathead tip in 100 mL volumes. The IR spectrum (Figure S1(a)) of the thus functionalized material is very similar to the IR spectrum of the functionalized sample prepared using the standard conditions (except more intense Mo–S vibrations). However, analysis of the XPS S 2p core level spectrum shows that the degree of functionalization is significantly lower (Figure S1(b)). This can be rationalized by a different power density (basically different effective energy input) in larger volume sonication because the ultrasonic intensity decreases both radially and axially from the ultrasonic probe.[2]

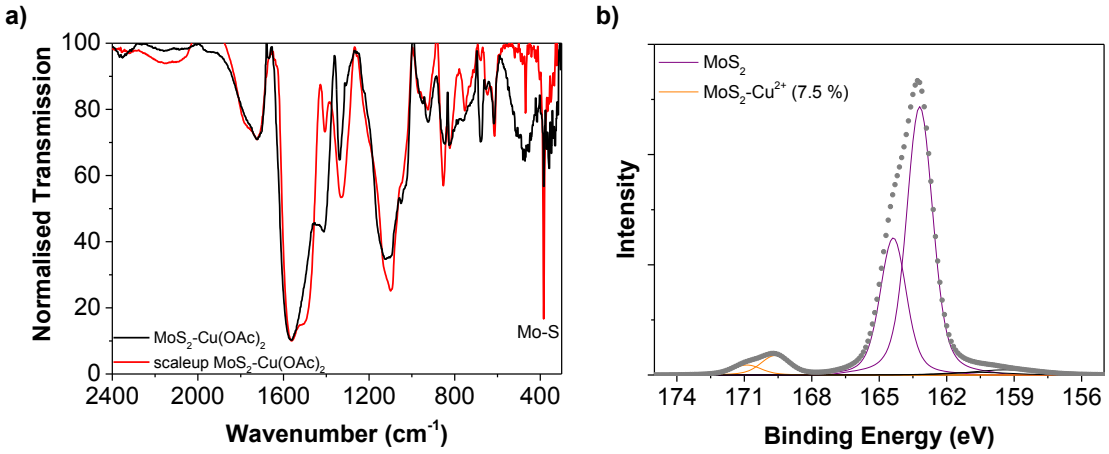

Figure S1: a) DRIFT-IR spectra of 2H-MoS_2-$Cu(OAc)_2$ prepared using a point probe sonic tip (black trace, low volume) and a flathead sonic tip (red trace, high volume). b) Fitted XPS S 2p core level spectrum of the flathead sonic tip prepared material.

Stability of the dispersions after functionalization

To test the stability of the $M(OAc)_2$ functionalized 2H-MoS_2, samples were subjected to optical extinction spectroscopy immediately after preparation and after 2 days. Potentially reaggregated 2H-MoS_2 was removed by low-speed centrifugation at 500 rpm (26 *g*). The optical extinction spectra display the characteristic excitonic transitions of 2H-MoS_2.[1, 3] In the case of the $Cu(OAc)_2$ functionalized samples (Figure S2(a and d)), these are superimposed on absorbance stemming from the salt. As shown in Figure S2(a-c), the concentration of 2H-MoS_2, i.e. the optical extinction, is significantly reduced after two days in the case of $Cu(OAc)_2$ (Figure S2(a)) and $Zn(OAc)_2$ (Figure S2(c)) functionalization, pointing to a pronounced reaggregation and destabilization of functionalized 2H-MoS_2. Interestingly, no such effect is observed in the case of the $Ni(OAc)_2$ functionalization (Figure S2(b)) suggesting that this is not due to reaggregation or destabilization by the increased ionic strength.

We also investigated whether different salt concentrations during the functionalization procedure have an impact on the stability of the dispersions. In Figures S2(d-f), we plot the extinction spectra of $M(OAc)_2$ functionalized 2H-MoS_2 using different salt concentrations in the mixture as indicated in the figure legends. The spectra are compared to the reference sample of 2H-MoS_2 after identical sonication and centrifugation conditions in the absence of salt. The reaggregation and destabilization in case of $Cu(OAc)_2$ (Figure S3(d)) and $Zn(OAc)_2$ (Figure S2(f)) functionalized 2H-MoS_2 is more pronounced for higher salt concentrations, i.e. the 2H-MoS_2 extinction systematically decreases with increasing salt concentration. This implies that the initial salt concentration provides a handle to vary the degree of functionalization in the samples. This is surprising, as in all cases, the salts are used in excess over the 2H-MoS_2. In analogy to Figure S2(b), no destabilization is observed in the case of the $Ni(OAc)_2$ functionalized 2H-MoS_2 (Figure S2(e)). In fact, the concentration in the functionalized sample is larger compared to the reference. This is due to an intrinsic destabilization of 2H-MoS_2 in IPA over time. We thus conclude that the $Ni(OAc)_2$ functionalization inhibits this reaggregation.

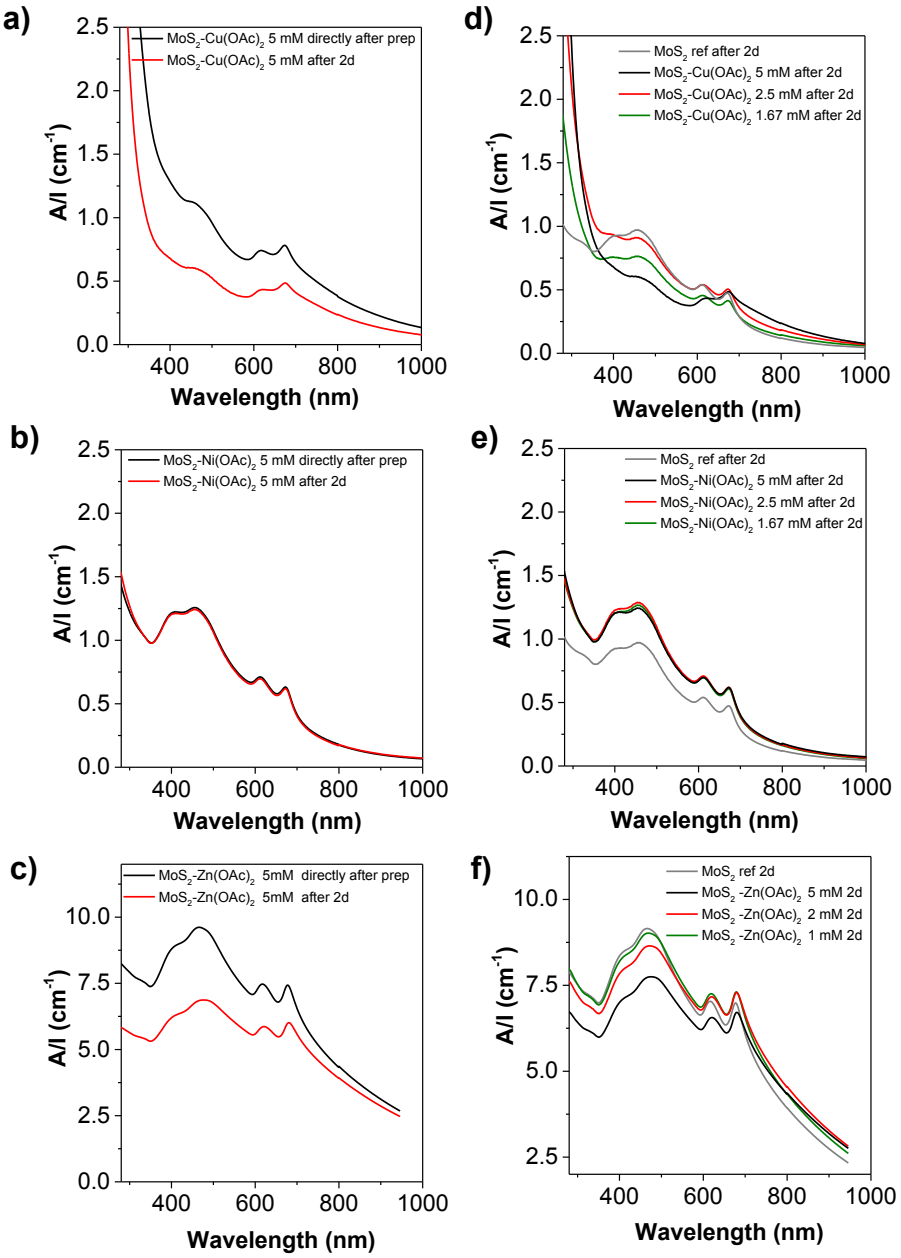

Figure S2: Optical extinction spectra of functionalized 2H-MoS_2 in 2-propanol. a, d) $Cu(OAc)_2$, b,e) $Ni(OAc)_2$, c,f) $Zn(OAc)_2$. a-c) Spectra obtained immediately after functionalization compared to spectra acquired after two days after removal of reaggregated material by centrifugation at 500 rpm . d-f) Extinction spectra of the dispersions of functionalized MoS_2 with different concentrations of the respective metal salt compared to the 2H-MoS_2 reference.

X-ray photoelectron spectroscopy

XPS is an extremely powerful tool to monitor functionalization. However, we note that it does not reflect the degree of bulk functionalization, as the technique is surface sensitive and our liquid-exfoliated 2H-MoS_2 is few-layered with a mean number of 9-10 layers. In XPS, the signal exponentially decays with the distance from the surface. In the case of our sample, we anticipated that the top few layers are probed. The degrees of functionalization reported here are an underestimate when considering the bulk material, but an overestimate when considering only the top layer.

In addition to the S 2p core level spectra, the coordination by $M(OAc)_2$ is further reflected in the Mo 3d core level spectra (Figure S3) that also show a clear additional component at higher binding energies in analogy to the S 2p core level spectra. However, due to a wider energy-splitting in the Mo $3d_{3/2}$ and Mo $3d_{5/2}$ doublet peaks, a partial overlap with the S 2s (also $M(OAc)_2$ @ S 2s) and intrinsically present MoO_x species, the spectra are more complex than the S 2p core level spectra. Even though the peak fitting convincingly shows the same trend in the degrees of functionalization (Table S1) as extracted from the S 2p core level spectra, a precise quantification is difficult (at least within the spectral resolution of our system). Unfortunately, the binding energy of the Mo 3d core level peaks in functionalized MoS_2 is very close to that of MoO_3 species that are intrinsically present in both the MoS_2 powder and sonicated MoS_2 (Figures S4). However, as we show below, this does not mean that the MoS_2 is oxidized during the functionalization.

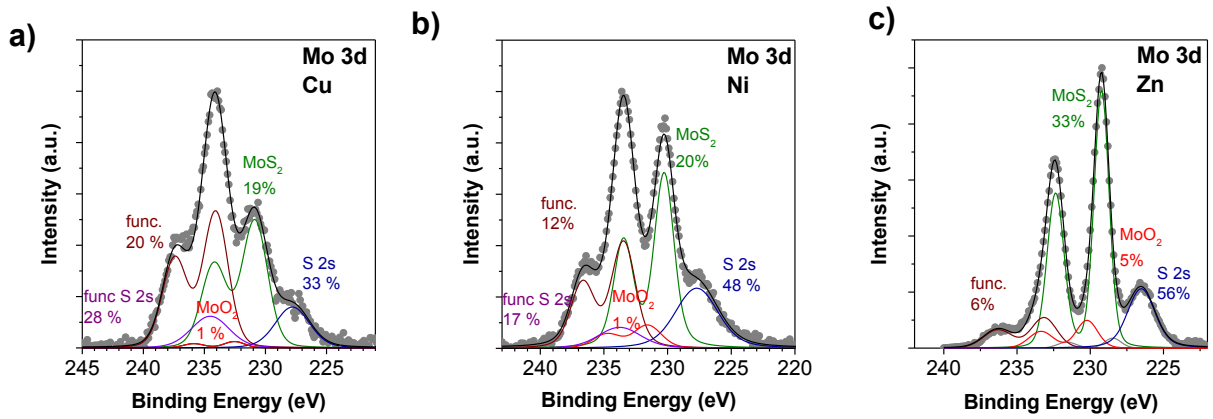

Figure S3: Fitted Mo 3d core level spectra of a) 2H-MoS_2-$Cu(OAc)_2$, b) 2H-MoS_2-$Ni(OAc)_2$, c) 2H-MoS_2-$Zn(OAc)_2$. The fit components and relative % are indicated in the figure. In total agreement with the S 2p core level spectra presented in the main manuscript, the coordination is also evidenced in the Mo 3d spectra. NB: features attributed to the functionalization overlap with MoO_3.

In addition, we note that the sonication did not result in an increased MoO_x content as shown by the Mo 3d and S 2p core level spectra of the untreated powder (Figure S4(a and c)) compared to the processed MoS_2 which was sonicated and exfoliated in IPA (Figure S4(b and d)). Note: The spectra of the untreated 2H-MoS_2 reference show much narrower peaks because they were acquired using the XPS system with a higher spectral resolution.

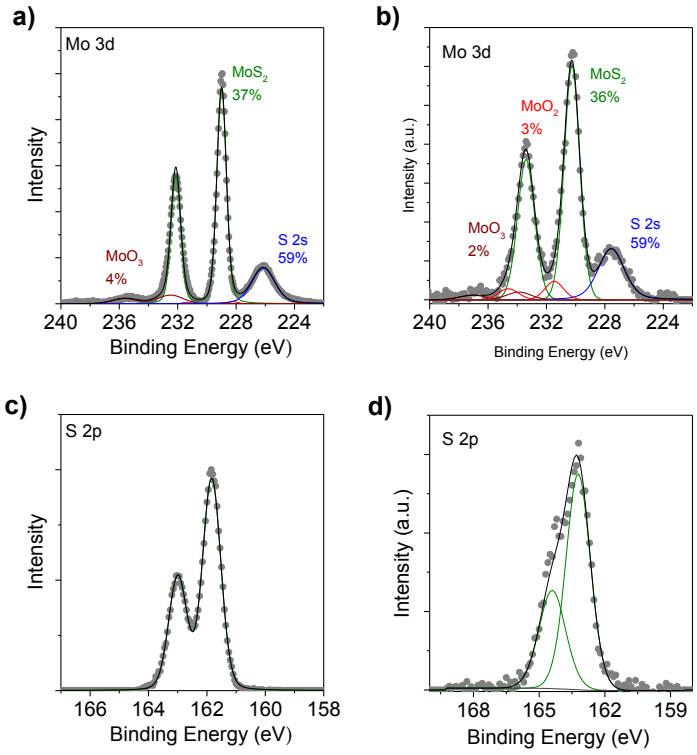

Figure S4: Fitted Mo 3d core level spectra (a, b) and S 2p core level spectra (c, d) of: untreated MoS_2 powder (a and c); and MoS_2 that was sonicated and exfoliated in 2-propanol (b and d). The processing did not result in oxidation of the material.

In addition to tracing changes in the chemical environment of a material by analysis of the XPS core level spectra, the XPS survey spectra can be used to determine the elemental composition at the surface of the material probed. The atomic percentages extracted from the XPS core level spectra for the untreated powder 2H-MoS_2, the sonicated 2H-MoS_2 reference, and the 2H-MoS_2-$M(OAc)_2$ are summarized in Table S1. Typically, the atomic percentage of M^{2+} is higher than the degree of functionalization determined from an analysis of the core level spectra suggesting that physisorption occurs in addition to coordination. We believe the physisorption occurs during the preparation of the materials for XPS analysis. It results in a greater than expected M^{2+} surface content in the functionalized materials. This is demonstrated in the XPS results suggesting 50% loading based on S 2p XPS spectra, and ~400% Cu loading based on survey spectra. We have analyzed all of our 2H-MoS_2-$Cu(OAc)_2$ materials (Graph S1) and we do not observe a correlation between the degree of physisorbed material and the degree of functionalized S-atoms. In addition, it is important to note that the atomic % of M from the XPS core level spectra is overestimated due to appearance of shake-

up peaks close to the core level, as has been described by Goodman.[4] In the same report, Goodman also highlights the fact that it is not possible to determine the oxidation state of Cu (or the other metals) from the XPS core level spectra because it has been shown that the Cu^{2+} is (partially) reduced to Cu^{+} by the X-ray irradiation during the XPS measurement. This prevents reliable measurement of the metal regions.

Accordingly, the degree of functionalization cannot be determined reliably from the survey spectra. In addition, carbon and oxygen levels found in the survey spectra cannot be used for quantification either since both elements can always be detected on 2H-MoS_2 films and most likely originate from adventitious C and contributions from the substrate filter paper to a varying extent.

We have furthermore analyzed the S:Mo stoichiometry based on both survey spectra and Mo 3d/S 2s core level spectra to test whether sulfur vacancies are introduced during the sonication and/or functionalization. The tabulated values are also summarized in Table S1. Even though we observe a lower S content than expected in all samples (it is always less than 2:1), we do not observe a significant change with sonication or functionalization. The S/Mo stoichiometry varies between 1.67 and 1.93 from the survey spectra and 1.6 and 2.4 from the Mo 3d/S 2s core level spectra. No trend is observed in the degree of functionalization and very often, the stoichiometry as determined from survey spectra and core level analysis significantly deviate. These results show that the error in determining stoichiometry from XPS is rather large (roughly ± 0.15 from survey and even higher from core level spectra) and that no systematic change in stoichiometry is observed.

Table S1: Atomic percentages according to XPS survey spectra after functionalization with $Cu(OAc)_2$, $Ni(OAc)_2$ and $Zn(OAc)_2$ and tabulated values of the degree of functionalization (per S atoms) according to S 2p and Mo 3d core level spectra as well as S:Mo stoichiometries.

	MoS_2 powder	**MoS_2 reference**	**$Cu(OAc)_2$**	**$Ni(OAc)_2$**	**$Zn(OAc)_2$**
Mo 3d	28.3 %	24.4 %	2.3 %	5 %	15 %
S 2p	47.2 %	43.3 %	3.9 %	8.8 %	29 %
C 1s	17.5 %	21 %	33.3 %	32.4 %	17.1 %
O 1s	6 %	7.9 %	44.6 %	46.4 %	31.5 %
Cu 2p3			16 %		
Ni 2p				7.5 %	
Zn 2p3					7.5 %
S/Mo from survey	1.67	1.77	1.69	1.76	1.93
S/Mo from core level	1.6	1.64	1.9	2.4	1.7
Degree of func. from S 2p			50 %	30 %	12 %
Degree of func. from Mo 3d			51 %	37 %	18 %

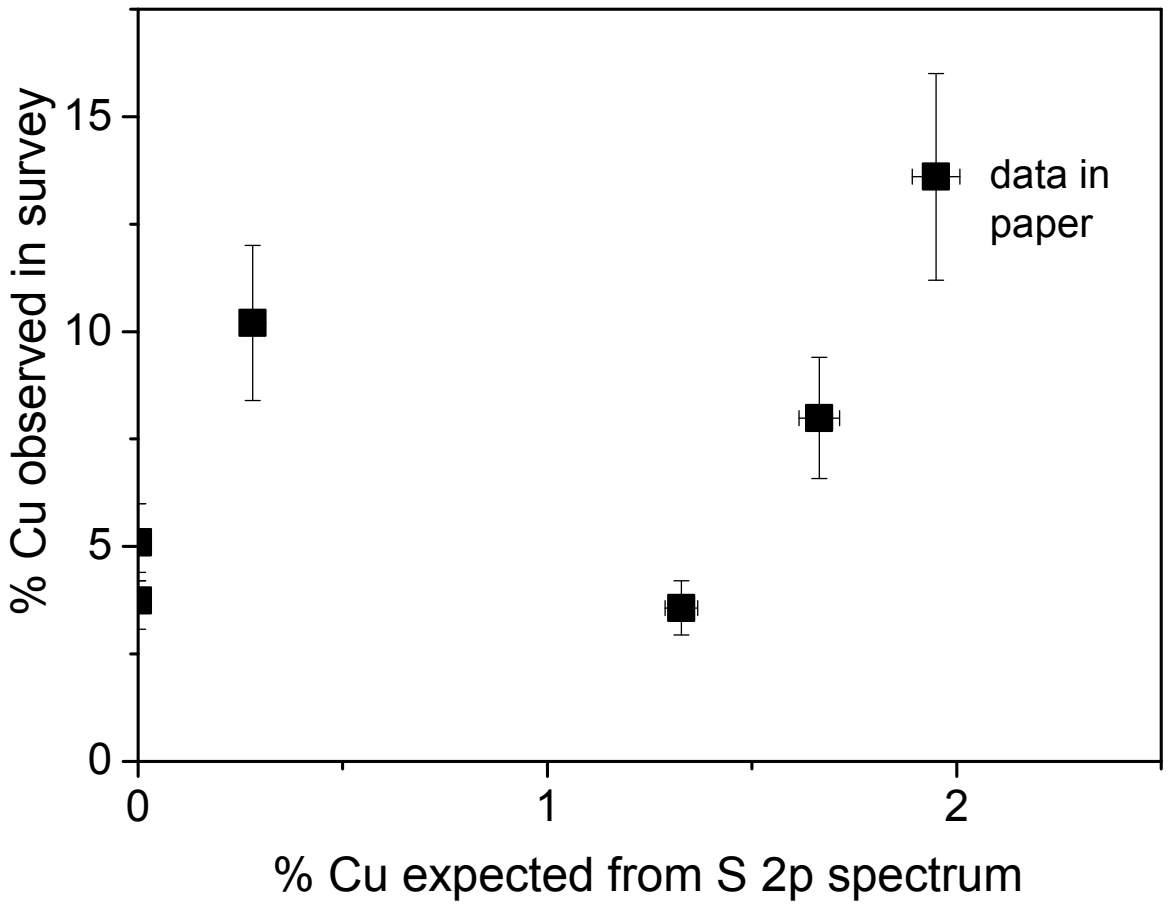

Graph S1. Comparison % of Cu from survey spectrum versus % of Cu expected from S 2p core spectrum (from 6 different preparations of 2H-MoS_2-$Cu(OAc)_2$). Demonstrates no trend in degree of physisorbed Cu versus coordinated Cu. The physisorbed Cu comes from poor washing of XPS samples.

As mentioned above, the Mo 3d core level region is very crowded and difficult to analyze with our limited resolution. However, it is important to confirm that no permanent structural disruption and/or oxidation of 2H-MoS_2 occurs during functionalization. As already briefly discussed in the main manuscript, we have thus attempted to defunctionalize the 2H-MoS_2-$Cu(OAc)_2$ in the mildest possible way. This is possible by a sequence of washing and bath sonication in NMP, as NMP is a coordinating solvent. For this purpose, the dried and functionalized 2H-MoS_2-$Cu(OAc)_2$ was redispersed in NMP by bath sonication in analogy to the redispersion experiment. In contrast to the redispersion study, all 2H-MoS_2 was removed from the dispersion by high-speed centrifugation (11,000 rpm). The supernatant was decanted and the sediment again redispersed in fresh NMP by 5 min bath sonication. This centrifugation-based washing cycle was repeated 4 times.

Figure S5 shows the Mo 3d and S 2p core level spectra of the 2H-MoS_2 reference (sonicated in IPA), the 2H-MoS_2-$Cu(OAc)_2$ and the defunctionalized sample in comparison. As most evident from the S 2p core level spectra in Figure S5(f), the repeated washing and redispersion in NMP results in a complete defunctionalization. The Mo 3d core level spectrum (Figure S5(c)) of this defunctionalized sample is virtually identical to the 2H-MoS_2 reference and does not show an increased content of MoO_x species further confirming that no permanent structural damage or rearrangement in induced by the $M(OAc)_2$ functionalization. NB: The spectra of the defunctiononalized MoS_2 were acquired using the XPS system with higher spectral resolution, yielding narrower peaks.

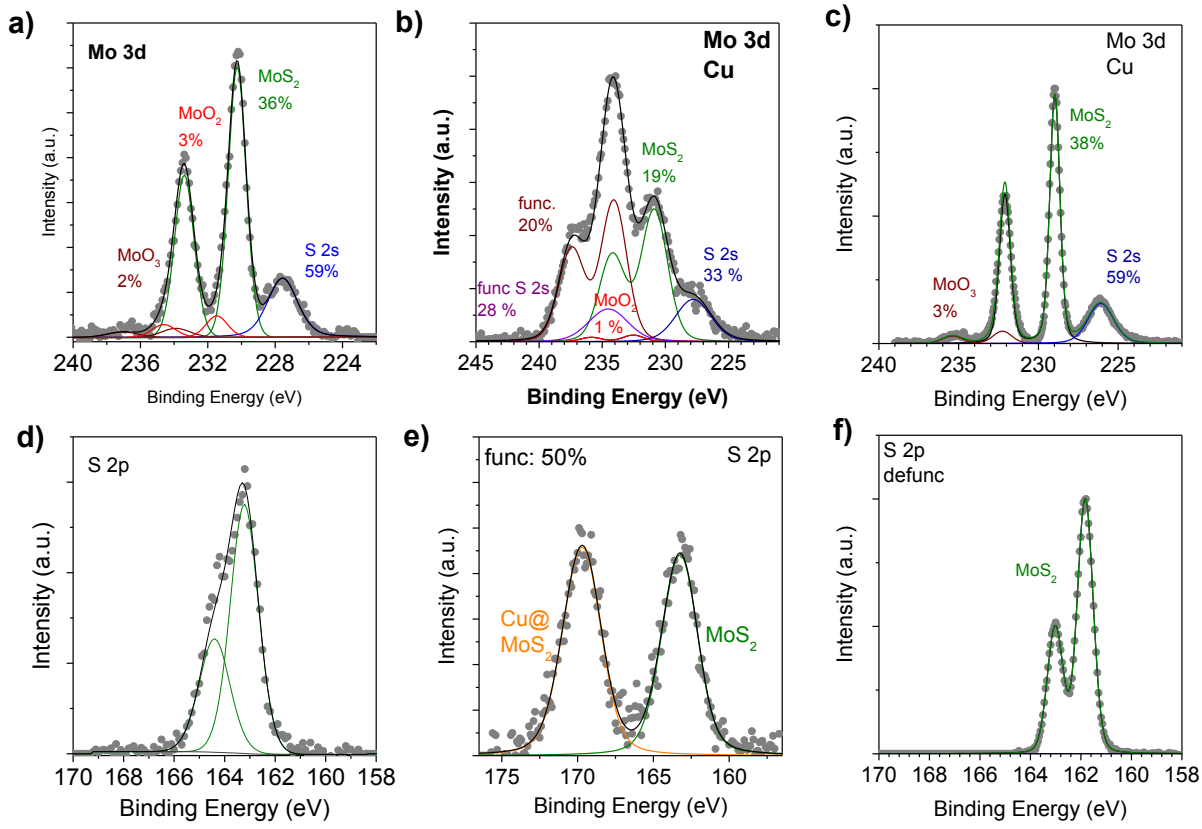

Figure S5: Fitted XPS Mo 3d/S 2s and S 2p core level spectra of: 2H-MoS_2 reference (a and d); 2H-MoS_2-$Cu(OAc)_2$ (b and e); defunctionalized 2H-MoS_2-$Cu(OAc)_2$ (c and f). NB: Mo 3d components attributed to the functionalization overlap with MoO_3.

Zeta Potential

To further analyze the oxidation state of the functionalized materials, we measured the zeta potential of 2H-MoS_2-$Cu(OAc)_2$ (Figure S6). The zeta distributions were very broad (due to low electrophoretic mobilities in solvents) and only showed negligible changes in the functionalized sample.

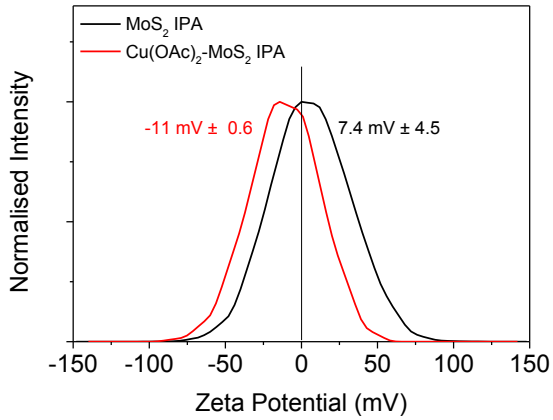

Figure S6: Zeta potential distributions of 2H-MoS_2 dispersed in IPA compared to 2H-MoS_2-$Cu(OAc)_2$. The mean of five measurements is displayed and the peaks are normalized for clarity.

DRIFT IR spectroscopy

Figure S7 shows the full DRIFT IR spectra of $M(OAc)_2$ and 2H-MoS_2-$M(OAc)_2$. The peaks in $Cu(OAc)_2$ were assigned according to reference [5]. Peaks for $Ni(OAc)_2$ and $Zn(OAc)_2$ were assigned accordingly. A zoom in of the low energy region of $Cu(OAc)_2$ and 2H-MoS_2-$Cu(OAc)_2$ is provided in Figure S8 and tabulated peak identifications are in Table S2.

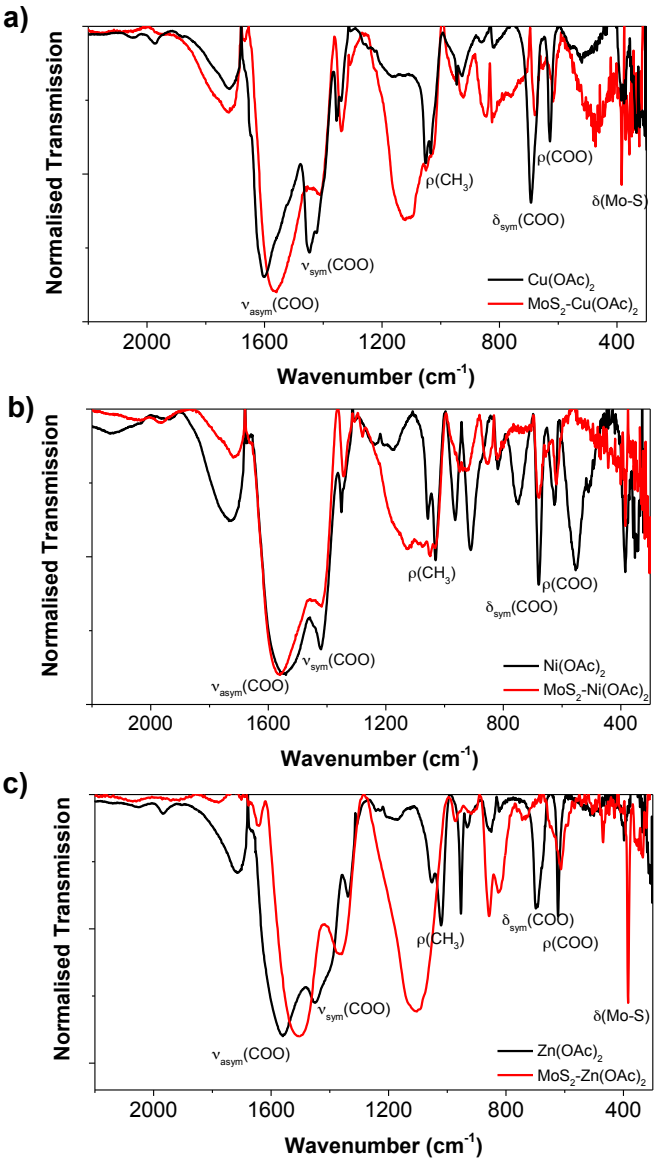

Figure S7: DRIFT-IR spectra (with CsI as matrix) of the pure metal salts and the functionalized 2H-MoS_2 products. In all cases, the acetate ligands can be clearly identified. The vibrations of the COO^- group are in general shifted to lower wavenumber when associated with the MoS_2 suggesting successful anchoring of the metal centres. a) $Cu(OAc)_2$, b) $Ni(OAc)_2$, c) $Zn(OAc)_2$.

In the pristine $Cu(OAc)_2$ salt, a number or vibrations we assign to Cu-O bonds appear in the low energy region (figure S8). In the functionalized MoS_2-$Cu(OAc)_2$ the δ(Mo-S) vibrations are clearly discernible at 470 cm^{-1} and 384 cm^{-1}, respectively.[6] We note that without isotopic labelling, a definite assignment of the peaks in the functionalized MoS_2-$Cu(OAc)_2$ is not possible.

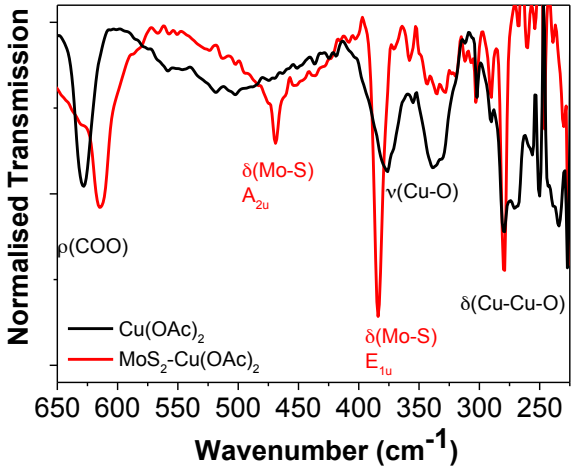

Figure S8: Low energy region of the DRIFT-IR spectra of $Cu(OAc)_2$ and MoS_2-$Cu(OAc)_2$.

Table S2: Tabulated values of the vibrational modes of $Cu(OAc)_2$ and 2H-MoS_2-$Cu(OAc)_2$ in comparison to literature data. All IR active vibrations associated with COO^- are shifted to higher energy.

	Literature [5] [cm^{-1}]	**MoS_2-$Cu(OAc)_2$ [cm^{-1}]**
ν_{asym}(COO)	1605	1565
ν_{sym}(COO)	1425	1410
δ_{sym} (CH3)	1356	1338
ρ(CH3)	1050	1050
ν(C-CH3)	935	920-940
δ_{sym} (COO)	690	675
ρ(COO)	625	616
ν(Cu-O)	377 330	Mo-S 384 332
δ(Cu-Cu-O_w)	272	280

Thermogravimetric analysis

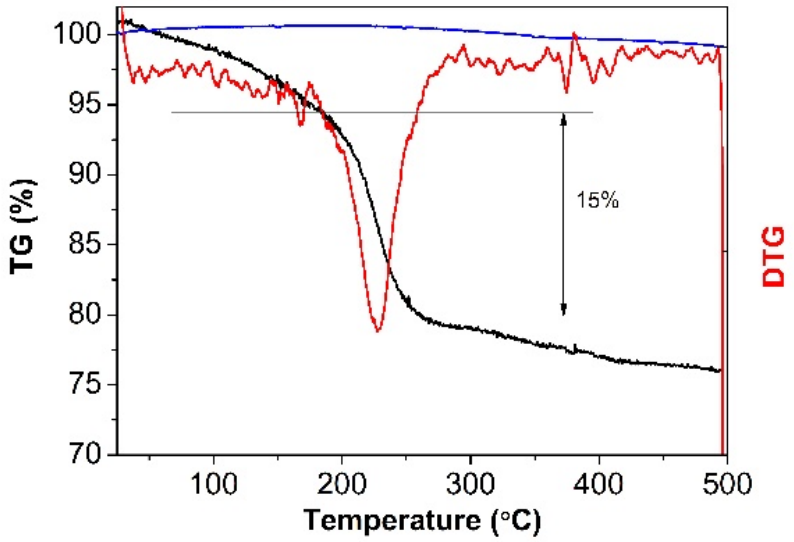

Figure S9: Thermogravimetric analysis (TGA) spectrum for 2H-MoS_2 (blue trace) and 2H-MoS_2-$Cu(OAc)_2$ (black trace).

IR and Raman spectroscopy after TGA

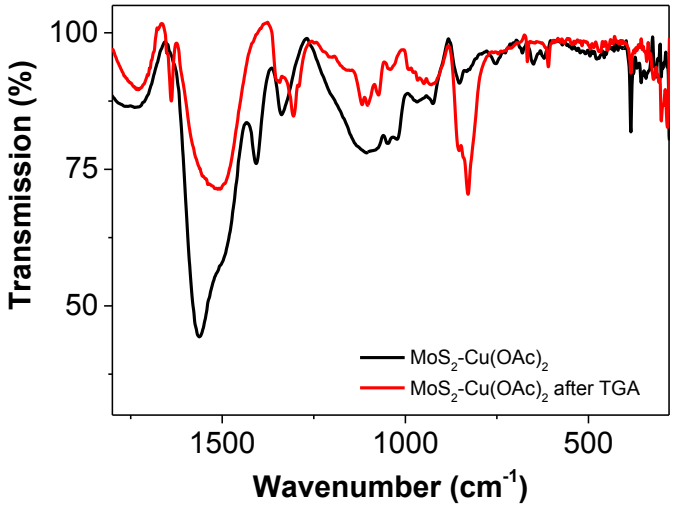

Figure S10. Comparison of DRIFT-IR spectra of 2H-MoS_2-$Cu(OAc)_2$ before and after TGA.

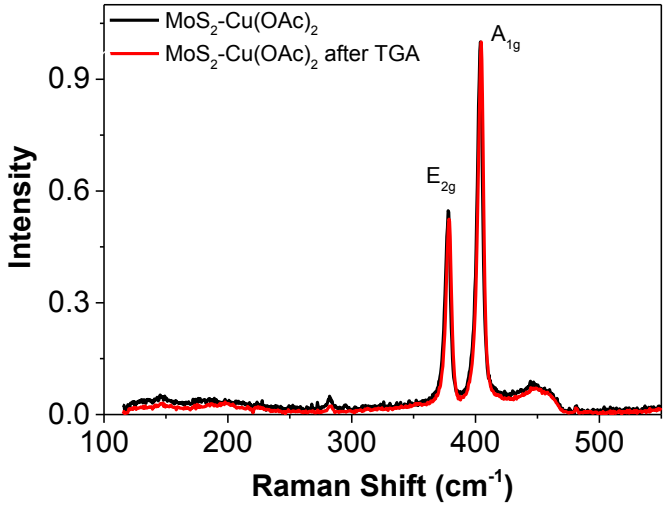

Figure S11. Raman spectra of 2H-MoS_2-$Cu(OAc)_2$ before and after TGA (excitation 532 nm) showing the characteristic MoS_2 phonons. No oxides were observed.[7]

References.

[1] C. Backes, R. J. Smith, N. McEvoy, N. C. Berner, D. McCloskey, H. C. Nerl, A. O'Neill, P. J. King, T. Higgins, D. Hanlon, N. Scheuschner, J. Maultzsch, L. Houben, G. S. Duesberg, J. F. Donegan, V. Nicolosi, J. N. Coleman, *Nature Communications* **2014**, *5*, 4576.

[2] Capelo-Martínez, José-Luis, *Ultrasound in Chemistry*, Wiley-VCH, Weinheim, **2008**.

[3] aJ. A. Wilson, A. D. Yoffe, *Advances in Physics* **1969**, *18*, 193-335; bJ. N. Coleman, M. Lotya, A. O'Neill, S. D. Bergin, P. J. King, U. Khan, K. Young, A. Gaucher, S. De, R. J. Smith, I. V. Shvets, S. K. Arora, G. Stanton, H.-Y. Kim, K. Lee, G. T. Kim, G. S. Duesberg, T. Hallam, J. J. Boland, J. J. Wang, J. F. Donegan, J. C. Grunlan, G. Moriarty, A. Shmeliov, R. J. Nicholls, J. M. Perkins, E. M. Grieveson, K. Theuwissen, D. W. McComb, P. D. Nellist, V. Nicolosi, *Science* **2011**, *331*, 568-571.

[4] C. C. Chusuei, M. A. Brookshier, D. W. Goodman, *Langmuir* **1999**, *15*, 2806-2808.

[5] Y. Mathey, D. R. Greig, D. F. Shriver, *Inorganic Chemistry* **1982**, *21*, 3409-3413.

[6] T. J. Wieting, J. L. Verble, *Phys. Rev. B* **1971**, *3*, 4286-4292.

[7] aS. Jimenez Sandoval, D. Yang, R. F. Frindt, J. C. Irwin, *Phys. Rev. B Condens. Matter* **1991**, *44*, 3955-3962; bC. Lee, H. Yan, L. E. Brus, T. F. Heinz, J. Hone, S. Ryu, *ACS Nano* **2010**, *4*, 2695-2700; cB. Windom, W. G. Sawyer, D. Hahn, *Tribol Lett* **2011**, *42*, 301-310.